



Title	Ultrasonic Soldering of Alumina to Copper Using Sn-Pb Solders(Materials, Metallurgy & Weldability)
Author(s)	Naka, Masaaki; Taniguchi, Hiroshi
Citation	Transactions of JWRI. 1991, 20(2), p. 259-264
Version Type	VoR
URL	https://doi.org/10.18910/10342
rights	
Note	

The University of Osaka Institutional Knowledge Archive : OUKA

<https://ir.library.osaka-u.ac.jp/>

The University of Osaka

Ultrasonic Soldering of Alumina to Copper Using Sn-Pb Solders†

Masaaki NAKA* and Hiroshi TANIGUCHI**

Abstract

Ultrasonic soldering was applied to join alumina to copper using Sn-Pb solders (0 ~ 100 mass % Pb). The intensity of ultrasound was 1 kW and 18 kHz. The joining mechanism was investigated by measuring the joining strength and analyzing the microstructure at interface of the joint.

First, Al_2O_3 was metallized by applying ultrasound in Sn-Pb solder bath. Then, the metallized Al_2O_3 was soldered with Cu using the same Sn-Pb solders. The ultrasonic wave effectively improves the wetting of molten Sn-Pb solders against alumina, and increases the strength of $\text{Al}_2\text{O}_3/\text{Cu}$ joint.

The strength of Sn-Pb solder itself dominates the strength of $\text{Al}_2\text{O}_3/\text{Cu}$ joints, and Sn-37 Pb solder which possesses the highest strength among the solders represents the maximum strength of joint.

KEY WORDS : (Ceramic - Metal Joining) (Ceramics) (Alumina) (Copper) (Ultrasonic Soldering) (Soldering) (Tin) (Lead)

1. Introduction

The molten alloys have been widely used as the fillers for joining of ceramics. The fillers have to possess the superior wettability against ceramics. Several methods were tried to improve the wettability. The alloying of active elements such as titanium effectively accelerates the wetting of molten copper and silver-copper based alloys^{1,2)}. The molten aluminum base alloys are also used as the filler metals for joining of ceramics, because the wettability of the alloys against silicon nitride is effectively improved by increasing the brazing temperature^{3,4)}.

The mechanical effect of ultrasonic wave other than the chemical effects of titanium and aluminum has been also tried⁵⁾. The ultrasonic wave effectively improves the wettability of molten zinc-base alloys against alumina, and the metallized alumina by applying the ultrasonic wave is joined to copper. Since the wettability of molten metals is improved using the ultrasonic wave, the joining temperature of ceramics to metals is also decreased. The decrease in the joining temperature definitely reduces the stress arising from the difference in thermal expansion between ceramic and metals.

This work tries, in successive from the previous one^{6,7)}, to improve the wettability of Sn-Pb filler metals during joining of alumina to copper by applying the ultrasound.

2. Experimental Procedure

Materials used were 99.62 mass% Al_2O_3 containing 0.1 mass% SiO_2 and others, and tough pitch copper containing 0.03 mass% O.

The size of materials was 6 mm in diameter and 4 mm in thickness. **Table 1** represents a series of composition for Sn-Pb filler metals. The phase diagram of the Sn-Pb filler metals⁸⁾ is shown in **Fig. 1**. **Figure 2** shows the process of ultrasonic brazing of ceramics to metal in Sn-Pb bath. Alumina was first metallized by applying the ultrasound in Sn-Pb solder bath. The intensity of ultrasound was 1 kW and 18 kHz. The soldering temperature and applying time of ultrasound were 473 to 573 K and 0 to 90 s, respectively. After metallizing alumina, alumina was lapped to copper metallized by applying the ultrasound in 3 s.

The joining strength of $\text{Al}_2\text{O}_3/\text{Cu}$ joints brazed with

Table 1 Chemical compositions of Sn-Pb solders used.

Sn-Pb	Pb(mass%)	Liquidus temperature (K)
Sn	0	505
Sn - 20Pb	20	472
Sn - 37Pb	37	456
Sn - 60Pb	60	509
Sn - 80Pb	80	553
Pb	100	600

† Received on October 31, 1991

* Associate Professor

** Graduate Student

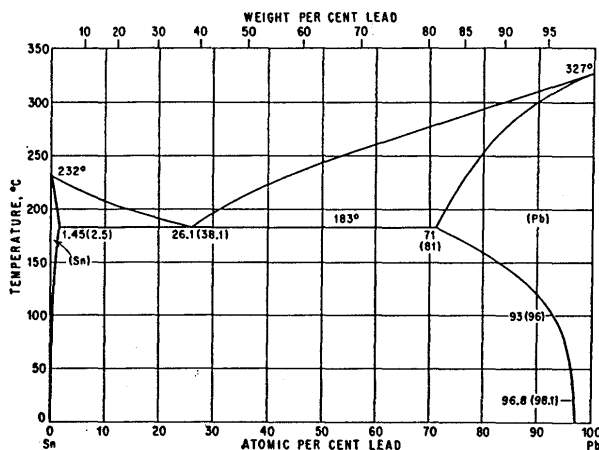


Fig. 1 Phase diagram of Sn-Pb Alloys.

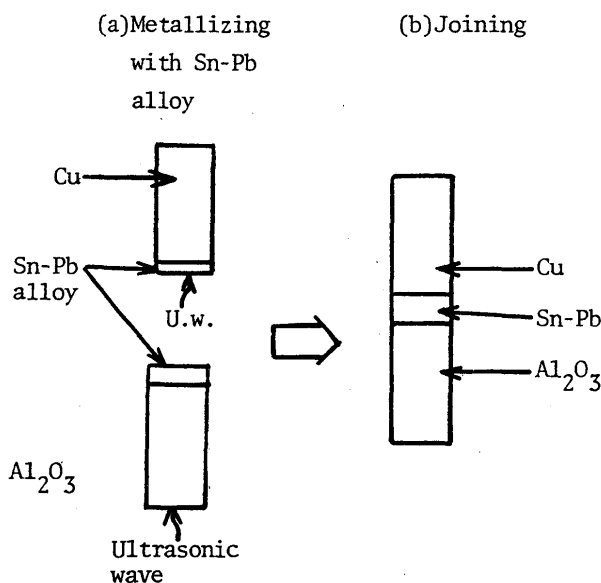


Fig. 2 Process of ultrasonic soldering of ceramics to metal.

Zn-Al filler was evaluated by fracture shear loading using a cross head speed of 1.67×10^{-2} mm/s, and the microstructure was analysed by scanning electron microscopy and EDX and EPMA microanalysis.

3. Results and Discussion

3.1 Joining strength of Al_2O_3 /Cu joint formed by ultrasonic soldering

Figure 3 shows the change in joining strength of Al_2O_3 /Sn-37Pb/Cu joint with application time of ultrasound. The application of ultrasound during brazing improves the strength of Al_2O_3 /Cu joining at all joining temperatures. For instance, the strength of the joint

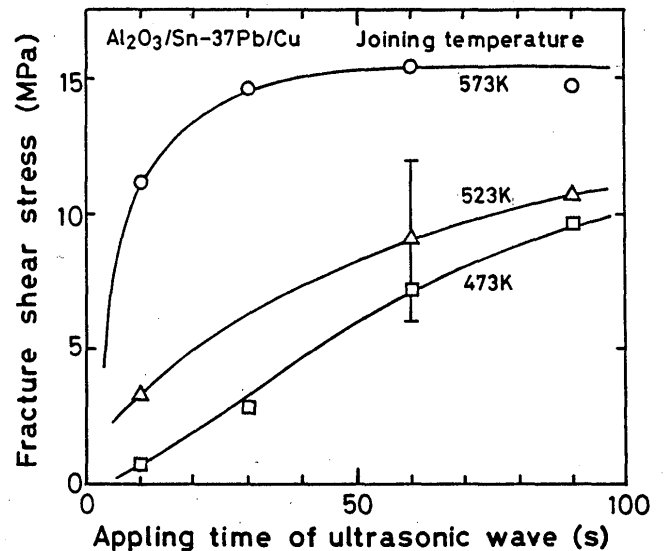


Fig. 3 Change in strength of Al_2O_3 /Cu joint using Sn-Pb solder with application time of ultrasound.

increases up to 12 MPa at 90 s with increasing the application time of ultrasound at joining temperature of 523 K, although the joint without applying ultrasound is not joined soundly.

The ultrasonic wave accelerates the motion of molten alloys in the filler bath and removes bubbles at the alumina-filler interface. Thus, the ultrasound improves the wetting of alloys against alumina. This results in the improvement of joining strength of Al_2O_3 /Cu joints.

The increase in joining temperature raises the joining strength at a constant applying time of ultrasound. Figure 4 represents the change in joining strength of Al_2O_3 /Cu joint using Sn-37Pb solder with joining temperature at the constant applying time of 60 s. The strength of joining changes from 6.5 MPa at 473 K to 16.5 MPa at 623 K at brazing condition of 60 s.

The change in joining strength of Al_2O_3 /Cu joint with Pb content in Sn-Pb filler at joining condition of 623 K and 60 s is shown in Fig. 5. The joining strength of Al_2O_3 /Cu joint increases with increasing Pb content in the filler from 11 MPa at 0 mass% Pb, and exhibits the maximum value of 17 MPa at 37 mass% Pb. With further adding Pb content, the strength lowers to 6 MPa at 100 mass% Pb through the maximum value.

Figs. 6 to 8 show the fracture surfaces of Al_2O_3 /Sn/Cu, Al_2O_3 /Sn-37Pb/Cu and Al_2O_3 /Pb/Cu joints soldered at 623 K for 60 s. The fracture of every joint takes place at the interface between Al_2O_3 and solder, and also at the solder. The solders exhibit the ductile fracture feature of adhering to Al_2O_3 . Since fracture feature is similar for every solder, the strength of solder itself dominates the strength of joint. The Sn-37Pb solder represents the highest strength among all solders as shown in Fig. 5.

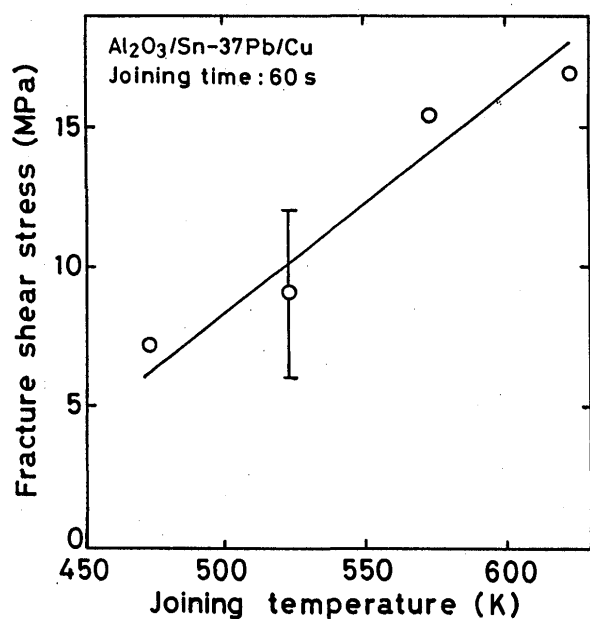


Fig. 4 Change in strength of $\text{Al}_2\text{O}_3/\text{Cu}$ joint using Sn-37Pb solder with joining temperature at application time of 60 s.

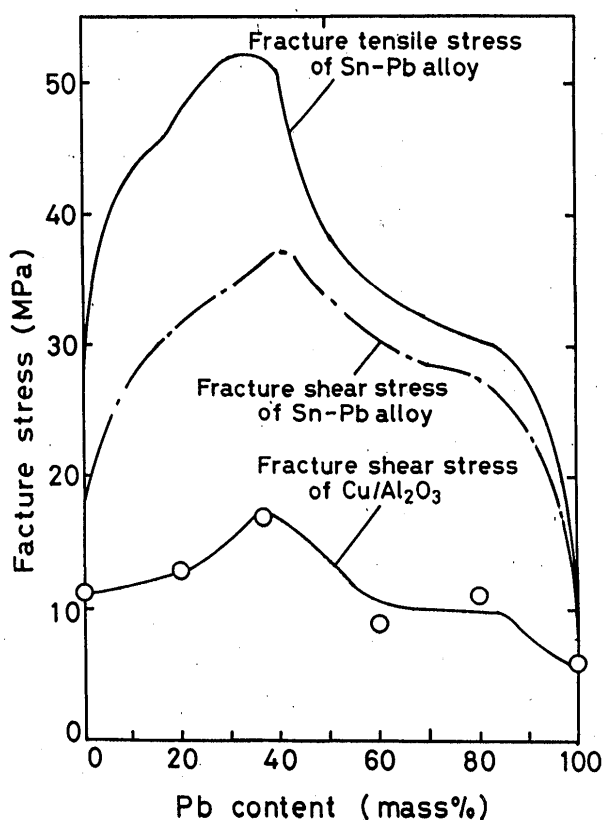


Fig. 5 Comparison of strength of Sn-Pb alloys with that of $\text{Al}_2\text{O}_3/\text{Cu}$ joints with Sn-Pb solders.

The dominating factor in strength of $\text{Al}_2\text{O}_3/\text{Cu}$ joint is also discussed in Fig. 8. In the figure the fracture strength of Sn-Pb alloys are compared with that of $\text{Al}_2\text{O}_3/\text{Cu}$ joint joined with Sn-Pb solder.

The fracture tensile stress and fracture shear stress of

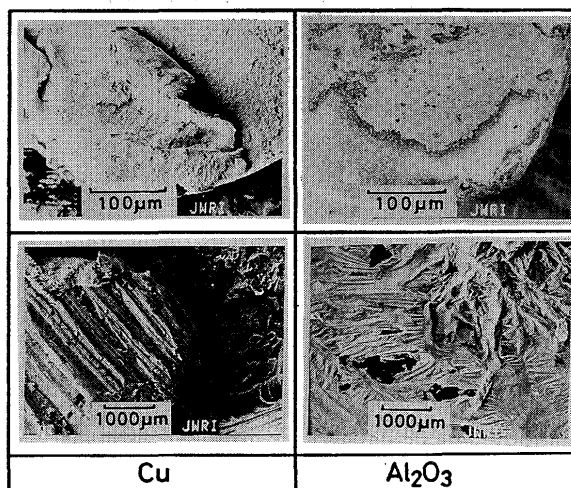


Fig. 6 Fracture surface of $\text{Al}_2\text{O}_3/\text{Sn}/\text{Cu}$ joint soldered at 523 K for 60 s.

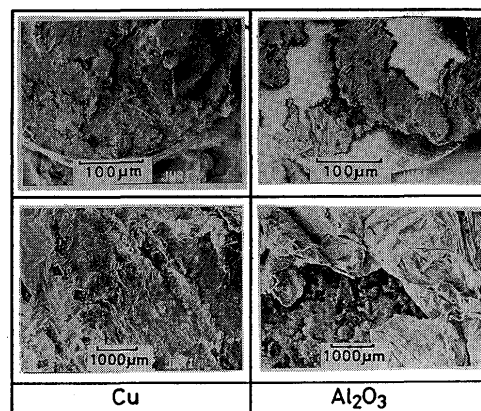


Fig. 7 Fracture surface of $\text{Al}_2\text{O}_3/\text{Sn-37Pb}/\text{Cu}$ joint soldered at 523 K for 60 s.

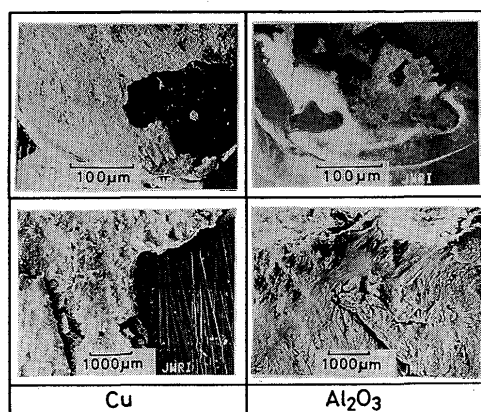


Fig. 8 Fracture surface of $\text{Al}_2\text{O}_3/\text{Pb}/\text{Cu}$ joint soldered at 523 K for 60 s.

Sn-Pb alloy are also plotted as a function of Pb content in the figure. The tendency in strength of Sn-Pb solder with Pb content gives the similar tendency of $\text{Al}_2\text{O}_3/\text{Cu}$ joint. In Fig. 9, the strength of $\text{Al}_2\text{O}_3/\text{Cu}$ joint joined with Sn-Pb solders is related with the strength of Sn-Pb solder. Sn-37Pb solder which possess the maximum strength gives

the highest strength of $\text{Al}_2\text{O}_3/\text{Cu}$ joint. These results imply that the strength of solder itself dominates the strength of $\text{Al}_2\text{O}_3/\text{Cu}$ joint.

Figure 10 shows the change in strength of $\text{Al}_2\text{O}_3/\text{Cu}$ joint using Sn, Pb or Sn-37Pb solder joined at 523 K for 60 s with testing temperature from room temperature to

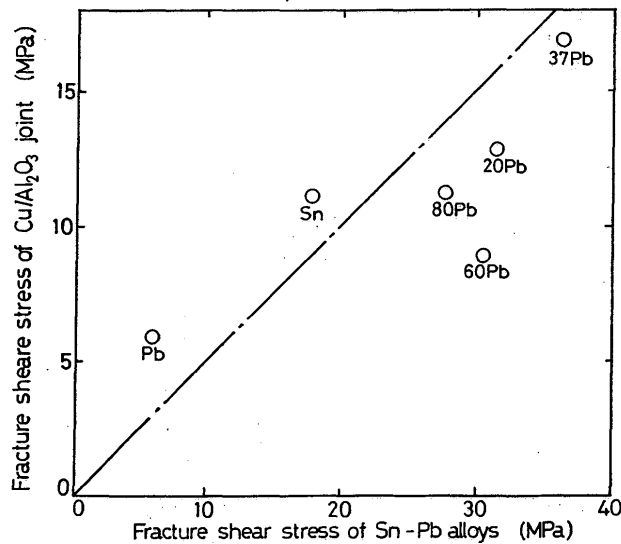


Fig. 9 Strength of Sn-Pb alloys plotted as a function of strength of $\text{Al}_2\text{O}_3/\text{Cu}$ joint joined with Sn-Pb solders.

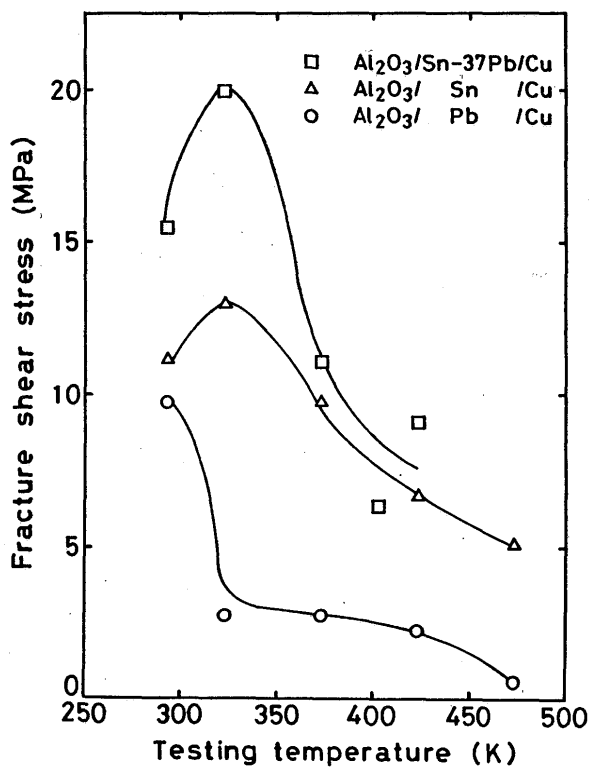


Fig. 10 Change in strength of $\text{Al}_2\text{O}_3/\text{Cu}$ joint using Sn, Sn-37Pb and Pb solders joined at 523 K for 60 s with testing temperature.

623 K. Sn-37Pb alloy among the three alloys represents

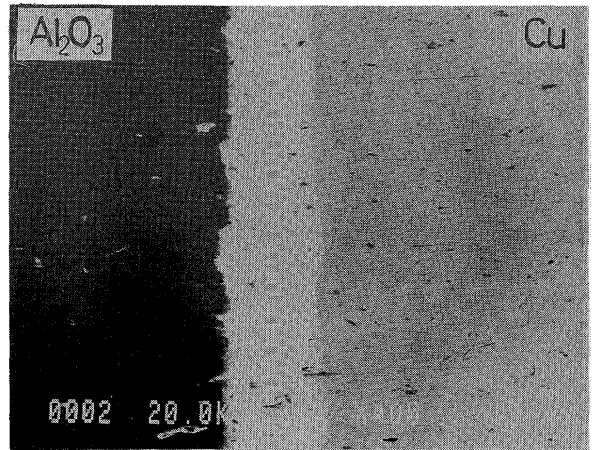


Fig. 11 Microstructure of $\text{Al}_2\text{O}_3/\text{Sn}/\text{Cu}$ joint soldered at 523 K for 60 s.

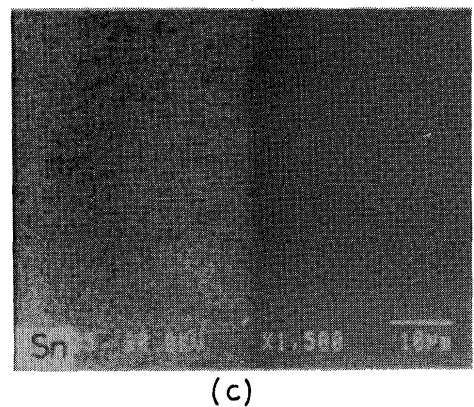
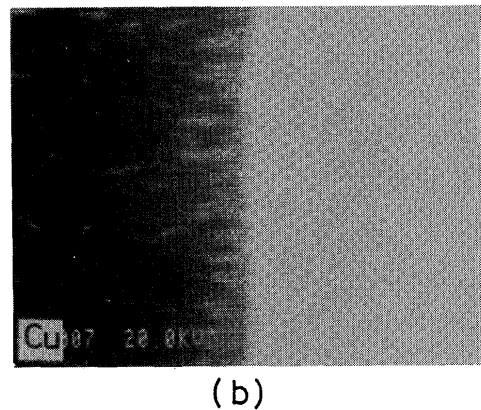
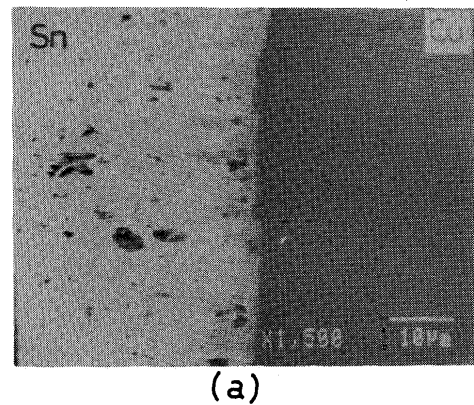


Fig. 12 Microstructure and X-ray image analyses of Cu and Sn of Sn/Cu interface of $\text{Al}_2\text{O}_3/\text{Sn}/\text{Cu}$ joint.

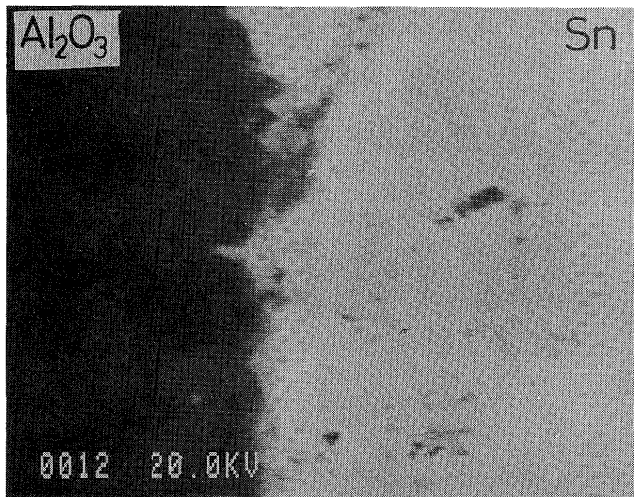
the highest strength at elevated temperatures.

The strength of Sn-37alloy exhibits the maximum at 323 K, and lowers with increasing temperature. The release of stress arising from the difference in thermal expansion coefficient is attributable to the increase in strength of joint at testing temperature of 323 K.

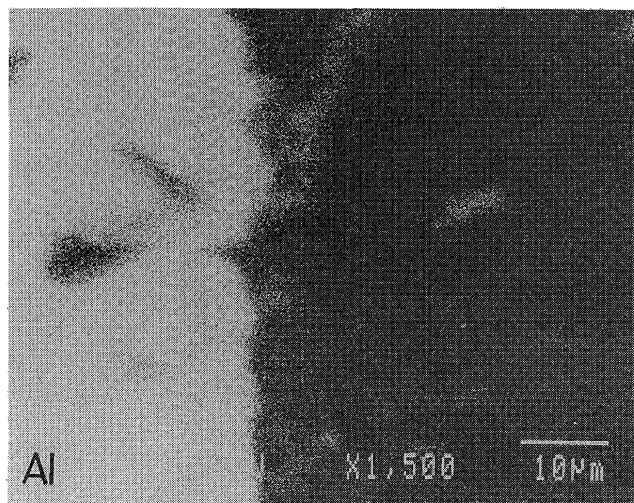
3.2 Joining microstructure at interface of $\text{Al}_2\text{O}_3/\text{Cu}$ joint

Figure 11 shows the microstructure of $\text{Al}_2\text{O}_3/\text{Sn}/\text{Cu}$ joint soldered at 523 K for 60 s. Sn well wets Al_2O_3 and Cu.

The microstructure, and X-ray image analysis of Cu and Sn in Sn/Cu interface of the joint are shown in Fig. 12. The Sn-Cu solid solution with 7.30 to 10 at% Cu is formed at the interface. The dendritic forms of solid solution suggest that the phase were formed into the molten solder.



(a)



(b)

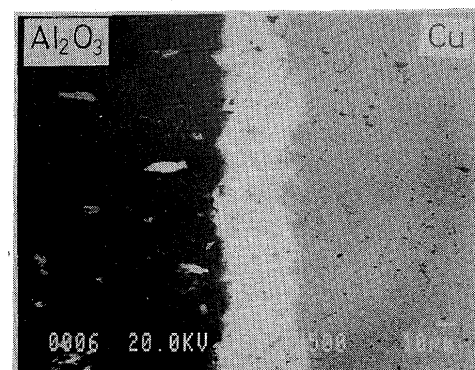
Fig. 13 Microstructure and X-ray image analyses of Al of $\text{Al}_2\text{O}_3/\text{Sn}$ interface in $\text{Al}_2\text{O}_3/\text{Sn}/\text{Cu}$ joint.

The microstructure and X-ray image analysis of Al of $\text{Al}_2\text{O}_3/\text{Sn}$ interface of the $\text{Al}_2\text{O}_3/\text{Sn}/\text{Cu}$ joint is shown in Fig. 13.

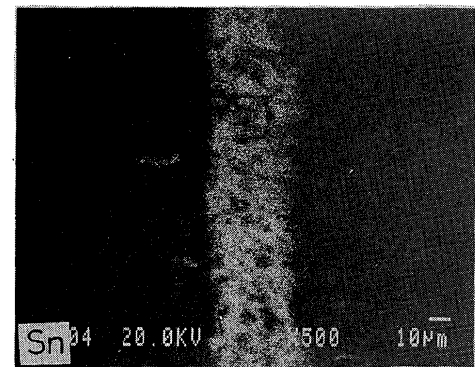
The aluminum distributes into Sn solder in Fig. 13(b). The ultrasonic wave operates to break alumina into the grains. Then fine alumina distributes into the Sn solder, and may dissolve into the solder.

Figure 14 represents the microstructure and X-ray image analysis of Sn and Pb in $\text{Al}_2\text{O}_3/\text{Sn-37Pb}/\text{Cu}$ joint soldered at 523 K for 60 s. The solders consist of Sn and Pb grains as shown in Fig. 14 (b) and (c). In contrast to the joint with Sn solder, the layer structure of Sn-Cu solid solution is not formed at solder /Cu interface.

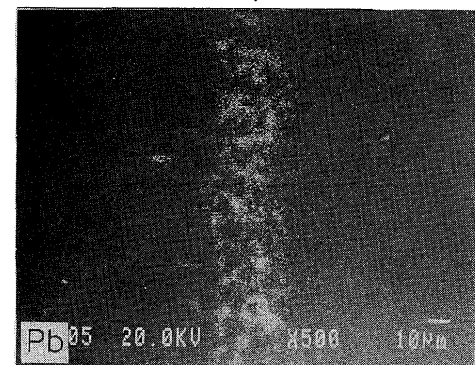
The microstructure of $\text{Al}_2\text{O}_3/\text{Pb}/\text{Cu}$ joint is given in



(a)



(b)



(c)

Fig. 14 Microstructure and X-ray image analyses of Sn and Pb in $\text{Al}_2\text{O}_3/\text{Sn-37Pb}/\text{Cu}$ joint soldered at 523 K for 60 s.

Fig. 15.

The alumina broken by applying of ultrasonic wave is shown in the Pb solder in the joint. This indicates that Pb solder is strongly agitated by ultrasonic wave and wets the alumina.

4. Conclusions

The joining of Al_2O_3 to Cu with Sn-Pb solders (0 ~ 100

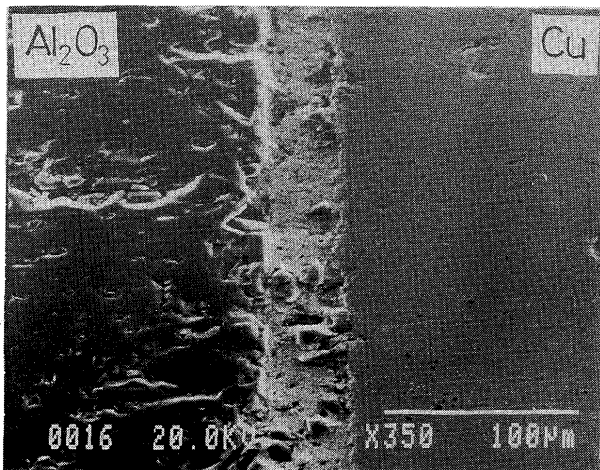


Fig. 15 Microstructure of $\text{Al}_2\text{O}_3/\text{Pb}/\text{Cu}$ joint soldered at 523 K for 60 s.

at% Pb) was conducted by ultrasonic soldering at 473 to 573 K and 0 to 90 s. The intensity of ultrasonic wave used was 1 kW and 18 kHz. The joining mechanism of ultrasonic soldering was investigated by measuring the joint strength and observing the microstructure of the interface of $\text{Al}_2\text{O}_3/\text{Cu}$ joint.

The ultrasonic wave strongly activates the motion of the solders and promotes the wetting of solder against alumina. This accounts for the increase in joining strength of the joint. The strength of Sn-Pb solder itself also dominates the strength of $\text{Al}_2\text{O}_3/\text{Cu}$ joint soldered. Sn-37Pb solder which possesses the highest strength provides the highest strength of $\text{Al}_2\text{O}_3/\text{Cu}$ joint.

References

- 1) M. Naka, T. Tanaka and I. Okamoto, Quaternary J. Japan Weld. Soc., 4 (1986), 113.
- 2) T. Iseki, H. Matsuzaki and J. K. Boadi, Am. Ceram. Soc. Bull. 64 (1985) 322.
- 3) M. Naka, M. Kubo and I. Okamoto, J. Mater. Sci. Letters, 6 (1987) 965.
- 4) M. Naka, M. Kubo and I. Okamoto, J. Mater. Sci., 22 (1987), 4417.
- 5) M. Naka and I. Okamoto, Metal-Ceramic Joints, ed. by M. Doyama and N. Iwamoto, MRS, 1989, 61.
- 6) M. Naka, M. Maeda and I. Okamoto, Trans. of JWRI, 18 (1989), No. 1, 75.
- 7) M. Naka and M. Maeda, Trans. of JWRI, 20 (1991), No.1, 91
- 8) M. H. Hansen, Constitution of Binary Alloys, 1958, p 1106.